separations

MDPI

*Article*

# Comprehensive Discovery and Characterization of Chemical Constituents in Huangqintang Decoction Using Off-Line Two-Dimensional Liquid Chromatography and High-Resolution Mass Spectrometry

**Yan Fang, Yi Nan, Xijie Tian, Junyu Zhang, Xiaojuan Chen, Juan Song, Haizhen Liang * and Baiping Ma ***

Academy of Military Medical Sciences, Beijing 100850, China
* Correspondence: lhzhcm@163.com (H.L.); mabaiping@sina.com (B.M.)

**Abstract**

Traditional Chinese prescriptions are characterized by complex chemical constituents and wide variations in constituent content, which pose a substantial challenge to their comprehensive characterization. As a classic traditional Chinese prescription known for its heat-clearing and detoxifying properties, Huangqintang Decoction (HQD) is composed of Scutellariae Radix, Paeoniae Radix Rubra, Glycyrrhizae Radix et Rhizoma, and Jujubae Fructus. In this study, we developed an off-line two-dimensional liquid chromatography that addressed the limitations of traditional analysis of unfractionated extracts, such as restricted peak capacity, which often obscured trace components. By coupling with ultra-high performance liquid chromatography-quadrupole time-of-flight mass spectrometry (UHPLC-Q-TOF/MS), this study successfully performed rapid identification or characterization of the complete chemical profile of HQD. Notably, beyond high-throughput identification, this approach leveraged characteristic fragment ions and reversed-phase chromatographic behaviors to differentiate some isomers of flavonoid glycosides and triterpenoid saponins, demonstrating its depth in structural identification. Flavonoid glycoside isomers were distinguished by diagnostic neutral losses, while flavanones and chalcones were characterized by retro-Diels–Alder (RDA) and β-rearrangement, respectively. Isomers of triterpenoid saponins were inferred from aglycone-specific pathways alongside RDA cleavages. Ultimately, a total of 192 compounds were identified, including 88 flavonoids, 80 triterpenoids, 7 monoterpene glycosides, 3 fatty acid amides, 3 phenylethanoid glycosides, 4 coumarins, 3 saccharides, 1 organic acid, and 3 others. This study demonstrated that the off-line two-dimensional liquid chromatography analysis strategy significantly enhanced chromatographic resolution and expanded the coverage of trace components. It presented an effective strategy for comprehensive compound identification in complex traditional Chinese medicine prescriptions.

**Keywords:** Huangqintang decoction; chemical constituents; isomer; off-line two-dimensional liquid chromatography analysis strategy; UHPLC-Q-TOF/MS

Check for updates

Academic Editor: Gavino Sanna

Received: 15 February 2026
Revised: 27 March 2026
Accepted: 29 March 2026
Published: 1 April 2026

**Copyright:** © 2026 by the authors. Licensee MDPI, Basel, Switzerland. This article is an open access article distributed under the terms and conditions of the Creative Commons Attribution (CC BY) license.

## 1. Introduction

Traditional Chinese prescriptions (TCPs) are a concentrated manifestation of the "holistic view" and "syndrome differentiation and treatment" concepts in traditional Chinese medicine (TCM). Their core lies in achieving coordinated integration and regulation

through multiple components, targets, and pathways by adhering to the formulation principles of "Jun (emperor)—Chen (minister)—Zuo (adjuvant)—Shi (courier)," thereby offering therapeutic advantages that single compounds do not possess [1,2]. However, it is precisely this complex design, grounded in holistic effects, that presents fundamental challenges to modern scientific research. The crux lies in how to systematically characterize a mixture sample characterized by complex chemical constituents and significant disparities in the content of its various components. The challenges in elucidating the material basis of TCPs significantly hinder the exploration of their pharmacological mechanisms and the improvement of quality control standards [3,4].

Huangqintang decoction (HQD) is a classic TCP for the treatment of heat-induced diarrhea and dysentery. It is first documented in the "Treatise on Cold Damage Disorders" (*Shanghan Lun* in Chinese) [5–7]. The prescription comprises Scutellariae Radix (*Scutellaria baicalensis* Georgi, Huang-Qin in Chinese, SR), Paeoniae Radix Rubra (*Paeonia lactiflora* Pall., Chi-Shao, PRR), Glycyrrhizae Radix et Rhizoma (*Glycyrrhiza uralensis* Fisch., *Glycyrrhiza inflata* Bat., *Glycyrrhiza glabra* L., Gan-Cao, GRR), and Jujubae Fructus (*Ziziphus jujuba* Mill., Da-Zao, JF) at a ratio of 3:2:2:2 [8–23]. According to the principle of formulation, SR serves as the emperor herb, PRR acts as the minister herb, GRR and JF function as the adjuvant and courier herbs. These four herbs work together to exert therapeutic effects. However, due to its complex components and significant differences in the content of various constituents, systematic research on the elucidation of the full chemical spectrum of HQD remains insufficient. Therefore, it is urgent to establish rapid and efficient methods for the characterization and identification of chemical components. This will not only help elucidate the material basis of their pharmacological effects but also hold significant value for deeply understanding the "holistic view" of TCPs.

Charged aerosol detection operates by detecting the charge of aerosol particles, where the charge amount is proportional to the analyte mass. As the detection signal exhibits a nonlinear response over a wide concentration range, the power function value algorithm is employed to transform this nonlinear response into a linear calibration curve, thereby enabling more accurate quantitative analysis [24,25]. For the problem of different ultraviolet absorption of components in TCPs, different detector signals such as ultraviolet (UV) and CAD can be used to trigger automated fraction collection, enabling precise isolation of specific components for further analysis [26]. The first-dimensional liquid chromatography ($^1$D LC) system integrates the HPLC platform with a vanquish fraction collector (VFC) and automated workflow. Through multi-detectors real-time monitoring and signal-triggered automated fraction collection, it enables complete process control from method development and sample analysis to target fraction collection. At its core, the system operates via an automated workflow of "real-time monitoring, intelligent triggering, and precise collection." The integrated LC-automated fraction collector and workflow enables accurate determination and optimization of the delay volume, ensuring synchronization between detection and collection, fundamental to high purity and recovery. To safeguard sample integrity, the system precisely controls fraction collection needle movement and employs various washing protocols to minimize cross-contamination, while the closed storage module with temperature and light control ensures fraction stability [27]. Thus, the $^1$D LC system can achieve the purpose of targeted removal of the main components in HQD and maintaining the integrity of trace components, laying the foundation for subsequent comprehensive component characterization and identification.

Ultra-high performance liquid chromatography coupled-quadrupole time-of-flight mass spectrometry (UHPLC-Q-TOF/MS) is characterized by high resolution, sensitivity, mass accuracy, and a broad scanning range [28,29]. By leveraging the accurate mass measurements and characteristic tandem mass spectrometry (MS/MS) information ob-

tained through MS/MS analysis, in conjunction with database searches, rapid structural elucidation of chemical constituents in TCPs can be achieved. In existing research, UHPLC-Q-TOF/MS technology has been applied to the chemical characterization of HQD. For instance, Sun et al. [30] identified 68 chemical constituents and 35 blood-absorbed components in HQD using UHPLC-Q-TOF/MS. Similarly, Tang et al. [31] tentatively identified 139 chemical constituents in HQD via UHPLC-Q-TOF/MS and revealed differences in metabolic profiles within an ulcerative colitis model. However, all these valuable studies are based on traditional analytical strategies, and their identification depth remains limited by strong interference from the complex matrix, manifested as co-elution of high-abundance components in chromatography and severe ion suppression effects in mass spectrometry. Consequently, although the major constituents of HQD have been partially characterized, its trace components, which are typically present at low abundance but may possess high biological activity, remain largely unexplored. These trace components may play a critical role in the synergistic therapeutic effects of TCPs, whose efficacy often arises from the combined action of multiple constituents rather than a single compound. Therefore, a comprehensive chemical profiling covering both major and trace constituents is essential for establishing a complete chemical basis for understanding the pharmacological mechanisms of HQD. To address this, the present study developed an innovative off-line $^{1}$D LC separation and second-dimension ($^{2}$D) UHPLC-QTOF/MS analysis combined strategy. The core advantage of this off-line $^{2}$D separation and analysis strategy lies in the targeted removal of main components, thereby achieving a significant enhancement in the identification rate of trace components. This approach enables the construction of a comprehensive chemical database for HQD and provides a powerful tool for investigating its pharmacodynamic material basis and multi-component synergy.

## 2. Results

### *2.1. Enrichment of Trace Components*

In this work, it was observed through CAD analysis that the HQD samples had a complex composition comprising multiple main components, which posed a challenge for comprehensive constituent analysis. By comparing the retention times and fragmentation characteristics with reference standards, seven main constituents in HQD were characterized, namely albiflorin, paeoniflorin, baicalin, wogonoside, wogonin, baicalein, and glycyrrhizic acid. Simply amplifying the response signals of the UHPLC-CAD chromatogram or increasing the sample injection volume did not effectively resolve the issue of the overall chromatographic peak abundance being affected by the prominence of the main components in HQD (Figure S1). Therefore, the $^{1}$D LC system was utilized to remove the main constituents and enrich the trace components in the sample, thereby achieving the characterization and identification of all constituents in HQD. Firstly, the chromatographic methods were systematically optimized to ensure suitable baseline separation with adequate resolution and stable peak shapes for multi-component detection. After fixing the column temperature at 35 °C and the injection volume at 1 μL, different chromatographic columns were evaluated under identical gradient elution conditions. Based on a comprehensive assessment of chromatographic peak separation (Figure S2A), the Agilent ZORBAX SB-C18 column was selected for subsequent analysis. The elution conditions were further optimized, as shown in Figure S2B. The optimized conditions were specified in Section 4.3. As shown in Figure S2(Bc), in the HPLC-CAD/UV system, seven main components in HQD could be preliminarily characterized, and these main components could achieve good separation. Based on the optimized conditions, the specific fraction collection strategy employed in this study was as follows: The start and end points of the target chromatographic peaks were identified by UV and CAD detectors, which generated trigger signals

to drive the fraction collection valve to switch within milliseconds. Within the specific time window defined by the trigger signal (RTs 8.10~8.75 min, 9.35~9.95 min, 24.20~25.50 min, 31.75~32.75 min, 37.5~39.00 min, 44.50~46.50 min, and 65.00~66.00 min), the chromatographic flow path was altered to direct the fraction containing the high-abundance dominant constituents to a specific sample vial, thereby achieving the targeted removal of the main components. Outside this time window, the system maintained the default flow path, continuously and completely collecting all remaining fractions enriched with trace components. These collected fractions were subsequently subjected to $^{2}$D UHPLC-Q-TOF/MS analysis. As shown in Figure 1A, the seven peaks with the highest peak areas were removed via the system, effectively enriching the remaining constituents. Consequently, the chromatographic peak richness was significantly enhanced, as demonstrated in Figure 1B.

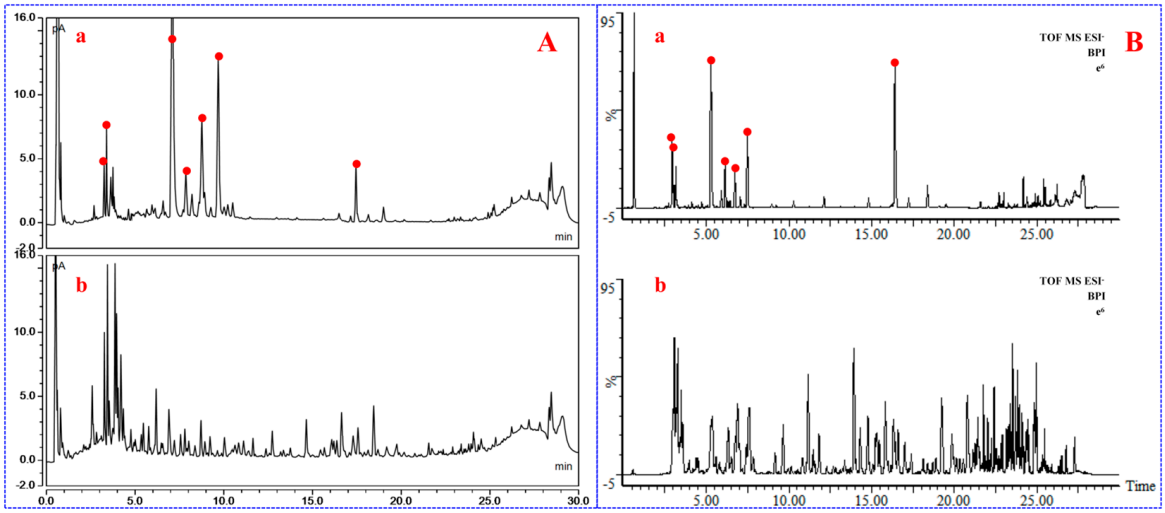



**Figure 1.** (**A**) UHPLC-CAD chromatograms of HQD before (**a**) and after (**b**) $^{1}$D LC system processing. (**B**) UHPLC-Q-TOF/MS chromatograms of HQD before (**a**) and after (**b**) $^{1}$D LC system processing. The seven main constituents are indicated by red dots.

### *2.2. Workflow of Chemical Constituents Identification in HQD*

Based on the optimized conditions, the chemical constituents of HQD were comprehensively identified and analyzed using $^{2}$D UHPLC-Q-TOF/MS analysis. A high-sensitivity data acquisition mode was employed to maximize MS/MS triggering for trace components. The base peak ion (BPI) chromatograms of HQD in both negative and positive ionization modes are presented in Figure 2A,B. Figures 3 and 4 present a summary diagram of the structural types of various constituents identified in HQD. According to the BPI profiles, compounds in HQD exhibited stronger intensity and greater abundance in negative ion mode compared to positive ion mode. To facilitate chemical identification, an in-house database was established, compiling information—including compound name, molecular formula, exact mass, and fragmentation patterns—of 1022 known constituents that have been reported for the four medicinal herbs of HQD. By integrating RT, accurate mass, MS/MS fragmentation behavior, and comparison with reference standards where available, a total of 192 compounds were identified or tentatively characterized. These comprised 88 flavonoids, 80 triterpenoids, 7 monoterpene glycosides, 3 fatty acid amides, 3 phenylethanoid glycosides, 4 coumarins, 3 saccharides, 1 organic acid, and 3 others. Among these 192 compounds, 11 were identified at Metabolomics Standards Initiative (MSI) Level 1, 146 were annotated at MSI Level 2.1, and 15 were tentatively characterized at MSI Level 2.2. Detailed information on these compounds was presented in the Supplementary Information Table S1.

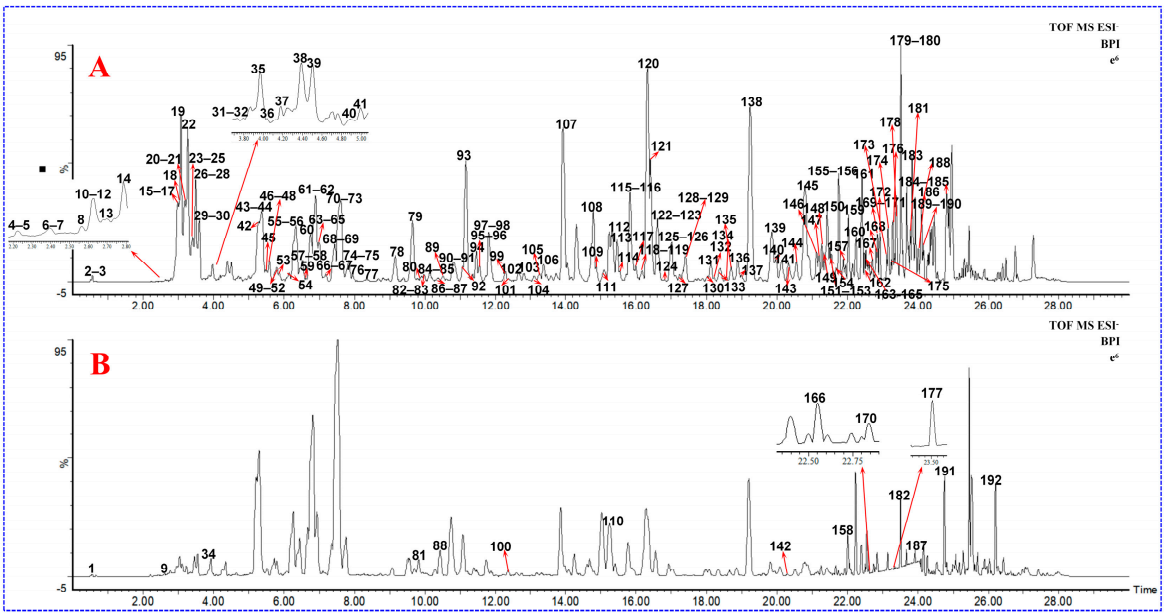



**Figure 2.** The qualitative analysis and comparisons on the chemical constituents of HQD by UHPLC-Q-TOF/MS. Base peak ion (BPI) chromatograms and the identification results in negative ion modes (**A**) and positive ion modes (**B**).

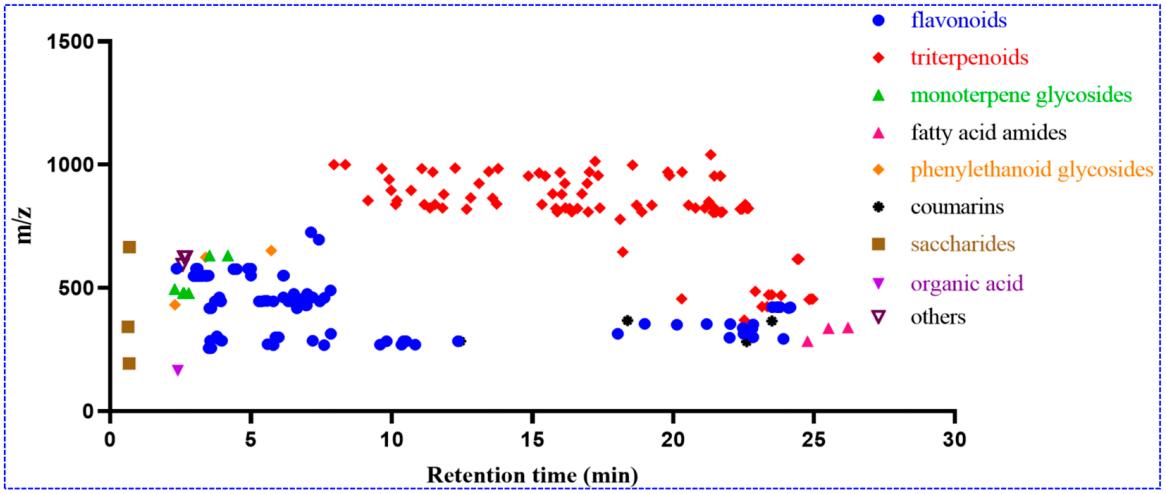



**Figure 3.** UHPLC-Q-TOF/MS-based qualitative analysis and comparison of the chemical constituents in HQD, summarizing the structural types of the identified compounds and presenting a 2D scatter plot (*m*/*z* vs. RT) of all 192 compounds.

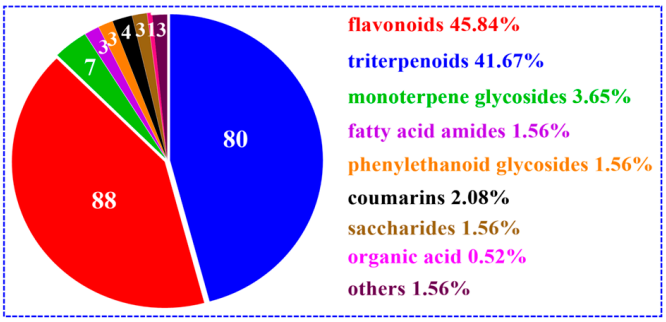



**Figure 4.** UHPLC-Q-TOF/MS-based qualitative analysis and comparison of the chemical constituents in HQD, summarizing the structural types of the identified compounds and presenting a pie chart illustrating the proportion of different component types.

2.2.1. Characterization of Flavonoid Constituents in HQD

HQD was found to contain a wide variety of natural constituents. Flavonoids were identified as the primary active components in HQD [32]. Previous studies have reported that flavonoids derived from HQD possessed antibacterial, anti-inflammatory, and hepatoprotective activities, which constituted the fundamental basis for the pharmacological activities of HQD [33,34]. Flavonoids predominantly existed in glycosylated forms. These compounds are combined with sugar molecules through glycosidic bonds via oxygen atoms (O) or carbon atoms (C), thereby forming different glycoside structures. This glycosylation not only improved their solubility and bioavailability but also modulated their pharmacological activity [35]. A total of 88 flavonoids were chemically identified or tentatively characterized in HQD, most of which originated from SR and GRR.

Taking compound **24** as an example, the compound **24** with an RT of 3.53 min presented a quasi-molecular ion peak at 417.1197 $[M-H]^-$ that was observed in negative ion mode. Therefore, the molecular formula was inferred to be $C_{21}H_{22}O_9$. The fragment ion at $m/z$ 255.0662 $[M-H-C_6H_{10}O_6]^-$ was generated by neutral loss of glucose residue with 162 Da from the parent ion. Then, RDA cleavage occurred, generating fragment ions with $m/z$ 135.0085 $[M-H-C_6H_{10}O_6-C_8H_8O]^-$ and $m/z$ 119.0500 $[M-H-C_6H_{10}O_6-C_7H_4O_3]^-$ (Figure 5A). Compared with our in-house database and reference standard, the compound was chemically defined as liquiritin [30]. As shown in Figure 5B, the quasi-molecular ion was observed at $m/z$ 445.0781 $[M-H]^-$, and the elemental composition was calculated as $C_{21}H_{18}O_{11}$, which further led to a series of product ions at $m/z$ 269.0453 $[M-H-C_6H_8O_6]^-$, 241.0503 $[M-H-C_6H_8O_6-CO]^-$ and 223.0401 $[M-H-C_6H_8O_6-CO-H_2O]^-$, resulting from the loss of one molecule of dehydrated glucuronic acid, CO, and $H_2O$ group in MS/MS spectrum. Comparison with the literature, in-house databases, and reference material identified compound **43** as baicalin [30].

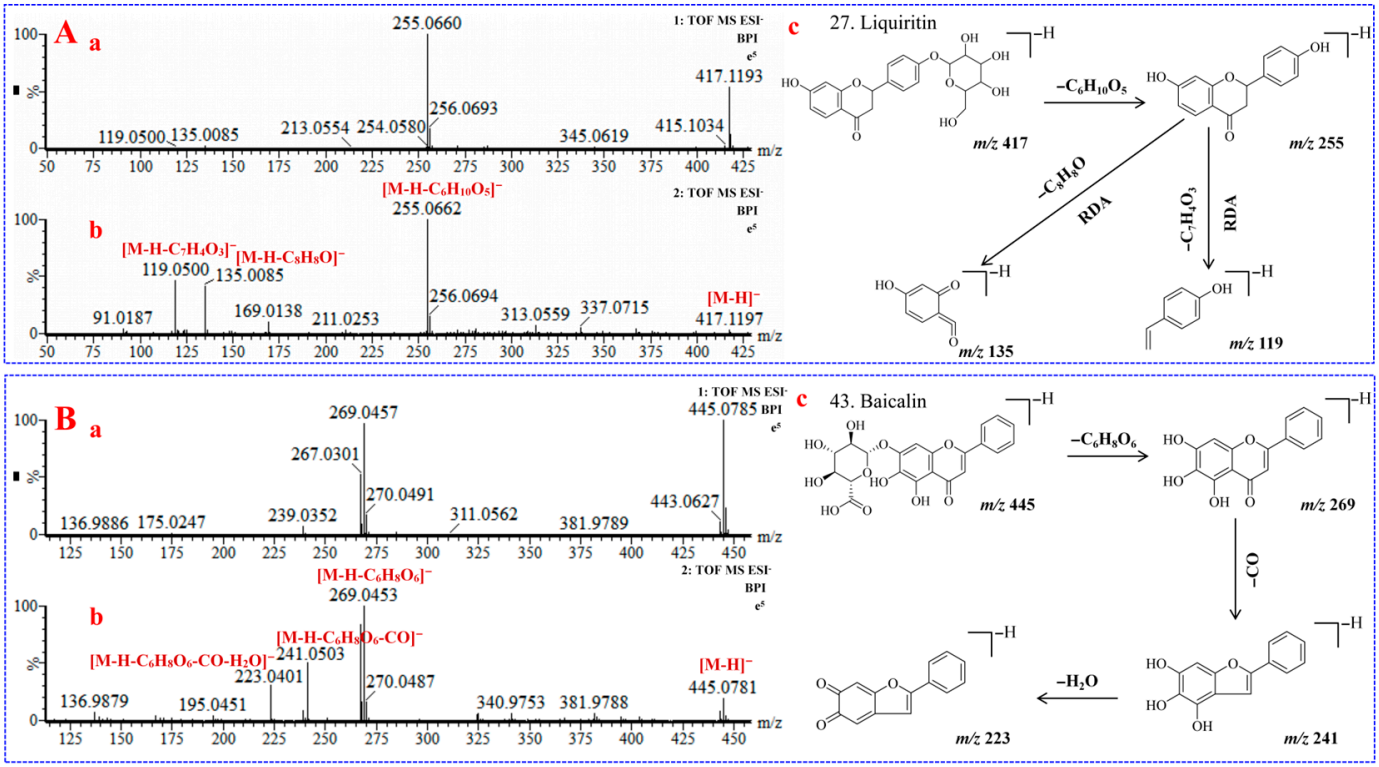



**Figure 5.** The MS1 (**a**), MS2 spectra (**b**) and characteristic fragmentation pathways (**c**) of liquiritin (**A**) and baicalin (**B**).

In addition, there were many isomers among the flavonoids in HQD. Based on the precise mass spectrometry fragment ions and the reversed-phase chromatography retention behavior, some isomers of flavonoid glycosides were identified and distinguished. Based on the analysis of the quasi-molecular ion peak, it could be calculated that the elemental composition of compounds **43**, **44**, **57** and **61** was all $C_{21}H_{18}O_{11}$. In the negative ion detection mode, the typical fragmentation patterns of flavonoid 7-*O*-glucuronides and 8-*O*-glucuronides are as follows: The 7-*O*-linked isomers undergo heterolytic cleavage of the glycosidic bond, resulting in the neutral loss of a glucuronic acid unit (176 Da) and the generation of an aglycone ion (*m*/*z* 269). In contrast, the 8-*O*-linked isomers undergo characteristic rearrangement fragmentation, preferentially losing a dehydrated glucuronic acid residue (148 Da) to form a key intermediate ion (*m*/*z* 297) [36,37]. Compound **44** presented characteristic dehydroxylation ion *m*/*z* 401.0542 and aglycone ion *m*/*z* 269.0452. Its key RDA cleavage fragment *m*/*z* 151.0554 clearly pointed to the apigenin aglycone, and combined with the typical 7-*O*-glycosidic bond cleavage pattern, it was identified as apigenin-7-*O*-glucuronide (Figure 6A). Compound **57** (RT 6.33 min) mainly generated the aglycone ion *m*/*z* 269.0450, accompanied by the characteristic fragment $[C_7H_3O_2]^-$ (*m*/*z* 119.2386) of the norwogonin B ring, which conformed to the 7-*O*-connection feature; therefore, it was putatively annotated to norwogonin-7-*O*-glucuronide (Figure 6B). Compound **61** (at 6.77 min) exhibited the characteristic rearrangement cleavage pathway at the 8-*O* position (producing *m*/*z* 297.0748 and its secondary fragment *m*/*z* 145.0282), and according to its longest retention time, it was putatively annotated to norwogonin-8-*O*-glucuronide (Figure 6C).

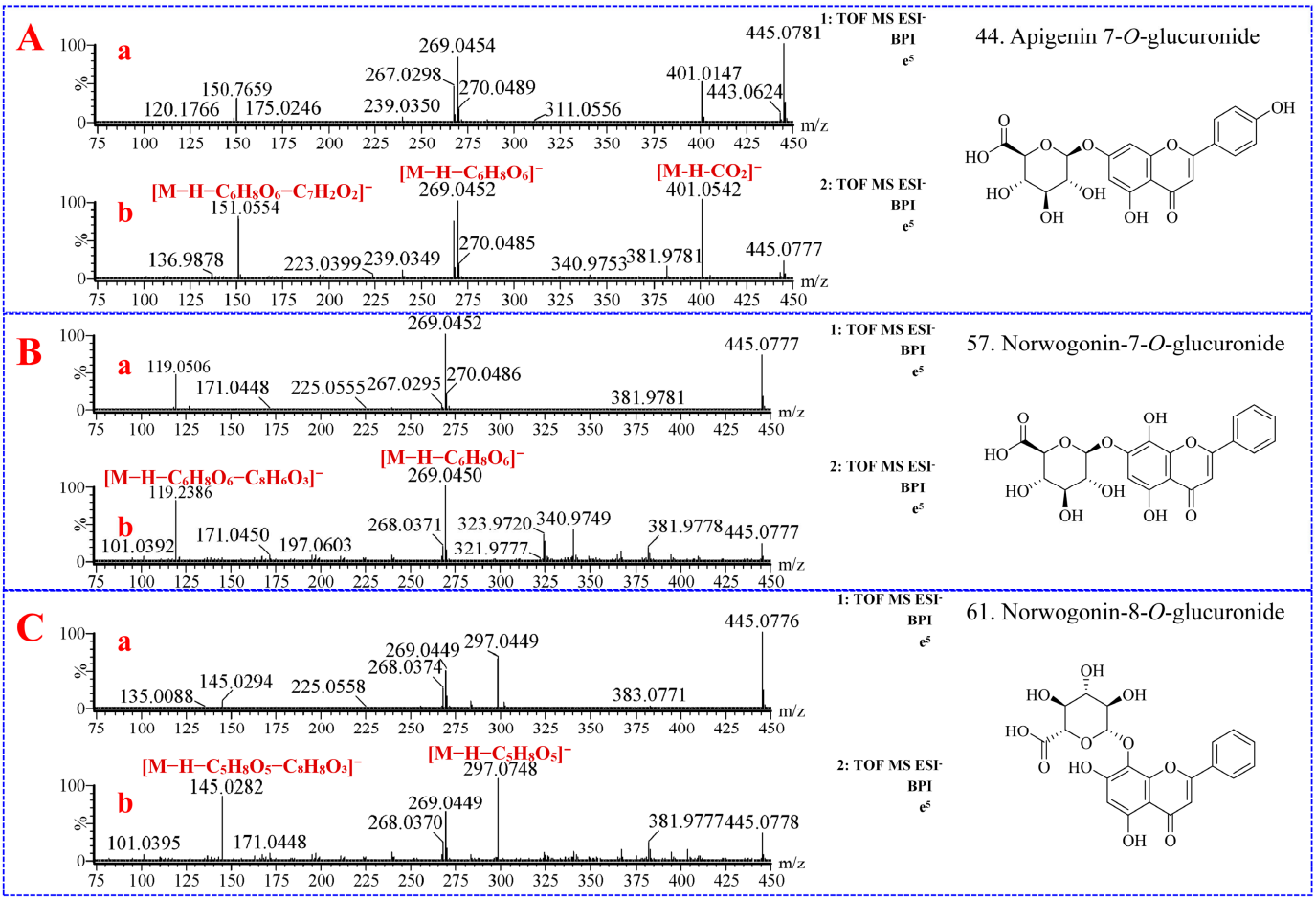



**Figure 6.** The MS1 (**a**) and MS2 spectra (**b**) of three isomers. (**A**) For apigenin 7-*O*-glucuronide, (**B**) for norwogonin-7-*O*-glucuronide and (**C**) for norwogonin-8-*O*-glucuronide.

Based on the quasi-molecular ion peaks, the elemental composition of compounds **21**, **24**, **42**, and **54** was inferred to be $C_{26}H_{30}O_{13}$. In negative ion mode, a series of deglycosylation fragments was observed for compounds **21** and **24**, including 417 $[M-H-132]^-$, 255 $[M-H-132-162]^-$, and 135 $[M-H-132-162-119]^-$. This indicated the successive loss of a pentose unit (132 Da), a hexose unit (162 Da), and a neutral $C_7H_3O_2$ fragment. This fragmentation pattern was consistent with the characteristic retro-Diels–Alder (RDA) cleavage of flavanone glycosides, which generates the diagnostic fragment ion $m/z$ 135 $[C_8H_7O_2]^-$. Additionally, extensive phytochemical studies on *Glycyrrhiza* plants have shown that the main flavanone glycosides are apiosylglucosides [38,39]. Therefore, it was deduced that the aglycones of compounds **21** (Figure 7A) and **24** (Figure 7B) were the liquiritigenin and that the attached sugar moieties were apiose and glucose. In contrast, apart from similar deglycosylation fragments, compounds **42** (Figure 7C) and **54** (Figure 7D) exhibited a prominent fragment at $m/z$ 147 $[C_9H_7O_2]^-$ in their MS/MS spectra, which is a characteristic ion generated from chalcone aglycones via β-cleavage and rearrangement of the enone skeleton. Combined with chromatographic behavior analysis, chalcone compounds, due to their larger conjugated system and stronger hydrophobicity, typically showed significantly longer retention times in reversed-phase chromatography compared to flavanones. It was inferred based on these differences that the aglycones of compounds **42** and **54** were the isoliquiritigenin. Furthermore, while both compounds **21** and **24** were identified as diglycosides of liquiritigenin, differences were observed in the abundance of their fragment ions derived from the aglycone ion ($m/z$ 255). The significantly higher abundance of the $m/z$ 135 fragment in compound **24** suggested that its A-ring structure remained intact and unsubstituted, facilitating efficient RDA cleavage. This observation aligned with the structural feature of the sugar chain being attached at the 4′-*O*-position on the B-ring. Additionally, when the sugar chain is linked to the B-ring, the hydrophobic part of the aglycone is more exposed, leading to slightly stronger chromatographic retention. Therefore, compound **24** was tentatively identified as liquiritigenin-4′-*O*-apiosylglucoside, and compound **21** as liquiritigenin-7-*O*-apiosylglucoside. Both compounds **42** and **54** were diglycosides of isoliquiritigenin, with the key distinction lying in the relative abundance of the characteristic fragment $m/z$ 147. The notably higher abundance of this fragment in compound **42** was consistent with the scenario where the 2′-hydroxyl group on the A-ring of isoliquiritigenin remains free. This free hydroxyl group can promote an intramolecular cyclization rearrangement via a neighboring group effect, making the formation of $m/z$ 147 the dominant fragmentation pathway. Based on this characteristic, the compound was putatively annotated as licraside, as reported in the literature [30]. In contrast, the relatively lower abundance of $m/z$ 147 in compound **54** suggested that its 2′-position was likely glycosylated, forming 2′-*O*-*β*-D-apiosyl-(1→2)-*β*-D-glucopyranosyl-isoliquiritigenin. Searches in SciFinder, PubChem, and related databases yielded no prior reports of this structure, leading to the tentative identification that compound **54** is a novel compound. Further structural validation by NMR would be required to confirm the novelty of compound **54**. The approach of utilizing characteristic differences in mass spectrometry and chromatographic behavior enables the systematic characterization and identification of positional isomers, encompassing both functional group isomers and glycosidic linkage isomers.

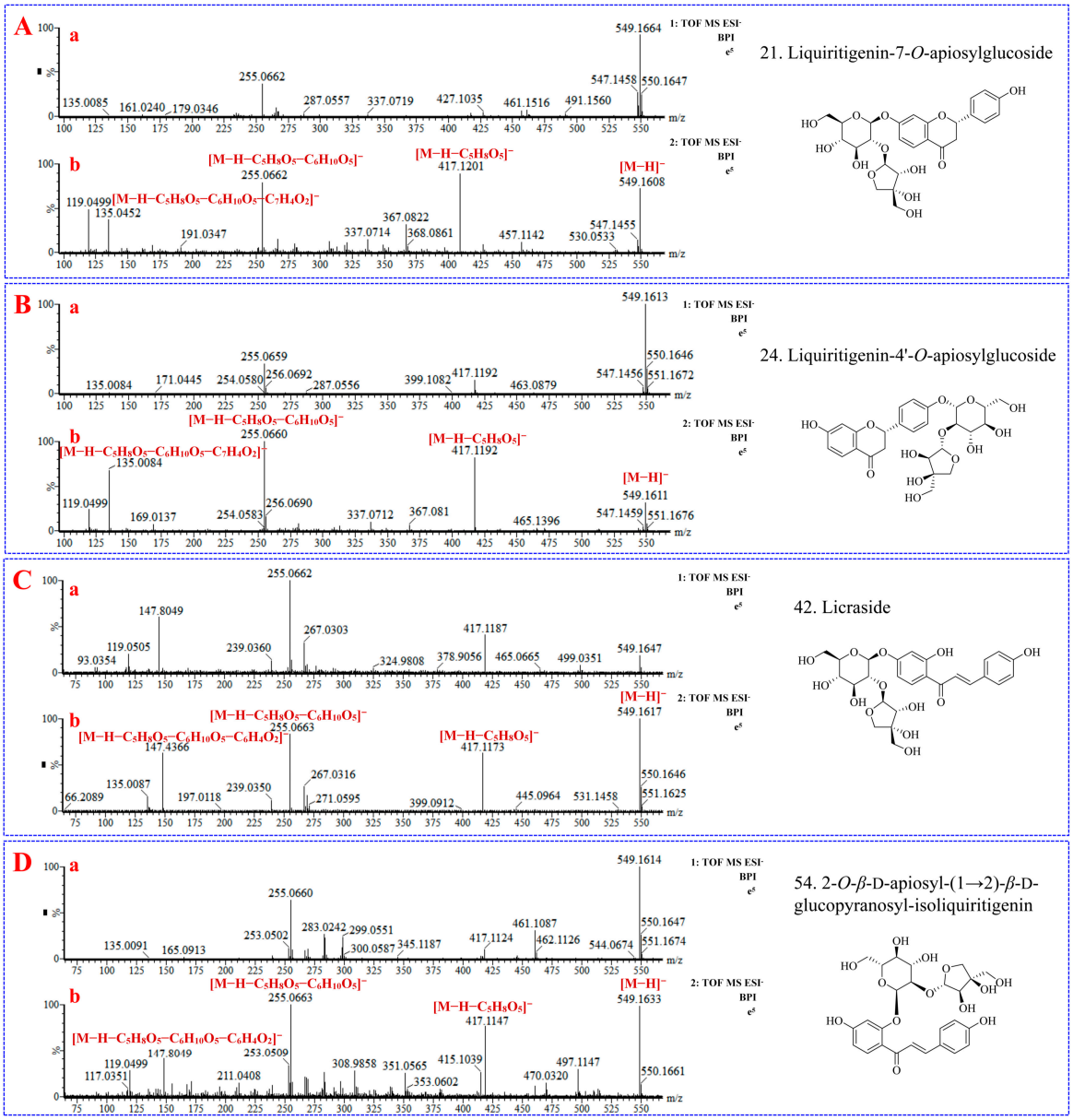



**Figure 7.** The MS1 (**a**) and MS2 spectra (**b**) of four isomers. (**A**) For liquiritigenin-7-*O*-apiosylglucoside, (**B**) for liquiritigenin-4′-*O*-apiosylglucoside, (**C**) for licraside and (**D**) for 2-*O*-*β*-D-apiosyl-(1→2)-β-D-glucopyranosyl-isoliquiritigenin.

### 2.2.2. Characterization of Triterpenoid Constituents in HQD

Triterpenoids have gathered significant attention due to their remarkable pharmacological activities. Studies reported that triterpenoids from HQD have anti-inflammatory and hepatoprotective activities [5,40]. In HQD, this class of compounds was predominantly characterized from GRR and JF, with a total of 80 triterpene derivatives identified, primarily consisting of oleanane-type and lupane-type categories. The fragmentation patterns of triterpenoid saponins usually involve the rupture of glycosidic bonds, leading to the formation of various aglycone ions. Licorice saponin A3 and glycyrrhizic acid were used to illustrate the identification process. A precursor ion of $[M-H]^-$ was observed at $m/z$ 983.4520, with a retention time of 9.65 min. In negative ion mode, collision-induced dissociation was performed, resulting in a series of secondary fragment ions, including $m/z$ 821.3993 $[M-H-C_6H_{10}O_5]^-$, $m/z$ 645.3651 $[M-H-C_6H_{10}O_5-C_6H_8O_6]^-$, and $m/z$ 469.3324 $[M-H-C_6H_{10}O_5-C_6H_8O_6-C_6H_8O_6]^-$. Based on the mass spectrometric data, it is suggested that the precursor ion $[M-H]^-$ first generated the fragment ion at

$m/z$ 821.3993 by the loss of one molecule of glucose. Subsequently, this fragment ion further lost one molecule of glucuronic acid, forming the fragment ion at $m/z$ 645.3651. Finally, the fragment ion at $m/z$ 645.3651 lost another molecule of glucuronic acid, resulting in the fragment ion at $m/z$ 469.3324. Comparing these data with existing literature and databases, compound **76** was identified as licorice saponin A3 [41]. The MS/MS mass spectrum of licorice saponin A3 is shown in Figure 8A. The precursor ion $[M-H]^-$, observed at $m/z$ 821.3987 at 16.33 min, underwent fragmentation to yield the ion at $m/z$ 351.0634, resulting from the neutral loss of glycyrrhetinic acid from the parent ion. Subsequently, the fragmented ion at $m/z$ 193.0355 was generated through the neutral loss of dehydrated glucuronic acid from the ion at $m/z$ 351.0634. Compared with our in-house database and reference standard, the compound was chemically defined as glycyrrhizic acid [30]. The MS/MS mass spectrum of glycyrrhizic acid is shown in Figure 8B.

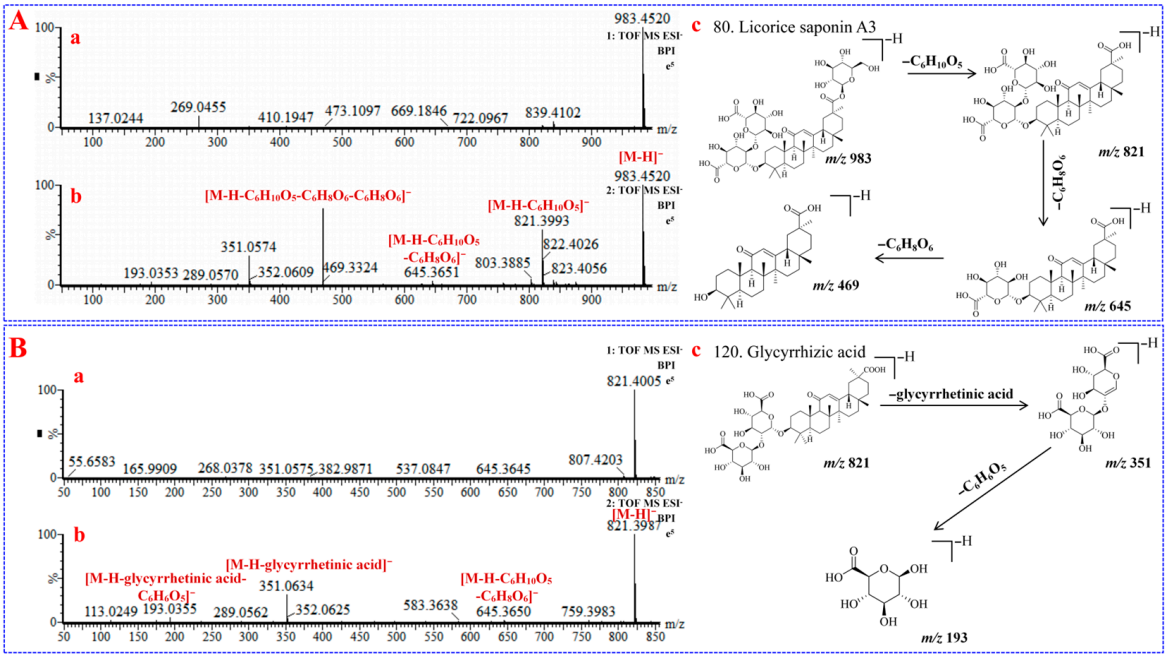



**Figure 8.** The MS1 (**a**), MS2 spectra (**b**) and characteristic fragmentation pathways (**c**) of licorice saponin A3 (**A**) and glycyrrhizic acid (**B**).

The data indicated that the molecular formulas of compounds **114, 120, 122, 167,** and **168** were all deduced to be $C_{42}H_{62}O_{16}$. Among them, compounds **114** and **122** generated characteristic fragment ions ($m/z$ 351 and 193) in the MS/MS mass spectrum that were identical to those of glycyrrhizic acid, leading to the inference that they are isomers of glycyrrhizic acid. In contrast, compounds **167** and **168** exhibited distinct fragmentation pathways. The mass spectrum of compound **167** (Figure 9A) was dominated by a decarboxylation loss, yielding a prominent $[M-H-CO_2]^-$ ion ($m/z$ 777.4104), while compound **168** (Figure 9B) mainly showed the rearrangement loss of $[M-H-CH_2O]^-$ ($m/z$ 791.3825) of the hydroxymethyl group. Further analysis revealed that their respective aglycone ions, generated after deglycosylation, continued these trends in secondary fragmentation: the aglycone from compound **167** underwent further $CO_2$ loss, while that from compound **168** underwent further $CH_2O$ loss. Based on these fragmentation signals, compound **167** was tentatively identified as Licorice saponin H2, which contains a carbonyl group at the C-11 position of its aglycone core, while compound **168** was putatively annotated as Licorice saponin K2, which contains a hydroxymethyl group at the C-4 position [41].

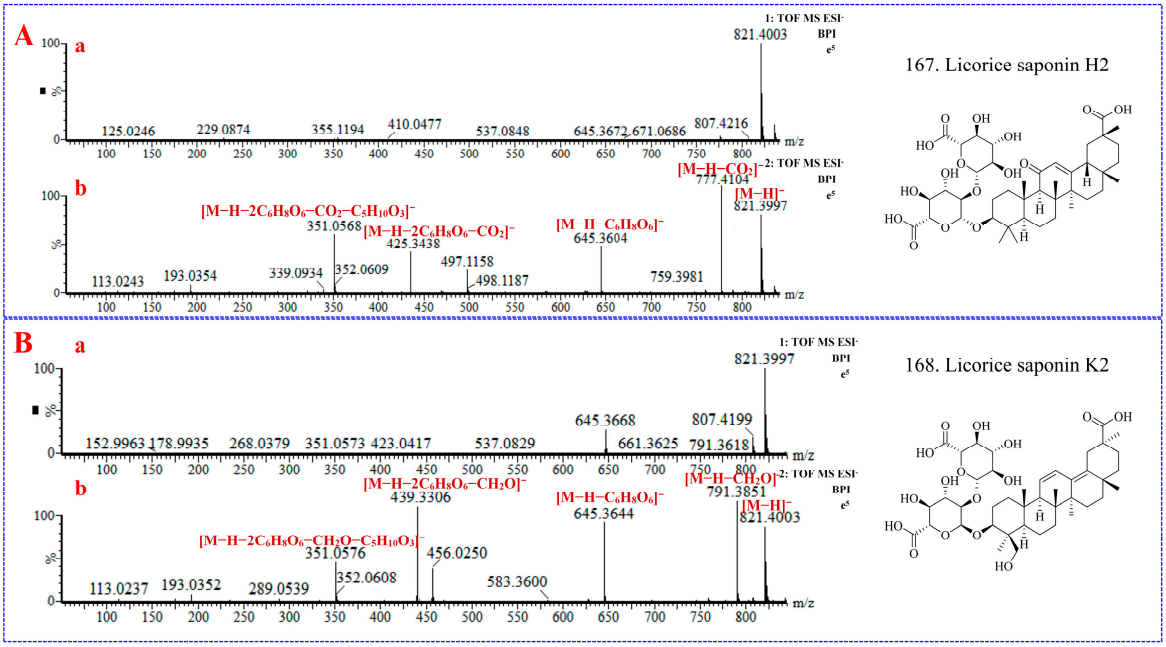



**Figure 9.** The MS1 (**a**) and MS2 spectra (**b**) of the two isomers. (**A**) For licorice saponin H2, and (**B**) for licorice saponin K2.

### 2.2.3. Characterization of Monoterpene Glycoside Constituents in HQD

Monoterpene glycosides are the most important type of active components in the medicinal herb PL of HQD. Pharmacological studies have shown that PL has multiple pharmacological effects, including anti-atherosclerosis, anti-diabetes, and anti-tumor activities [42]. Paeoniflorin and galloylpaeoniflorin are representative monoterpene glycosides found in PL, which are used to illustrate the identification process.

The precursor ion $[M-H]^-$ with an $m/z$ of 479.1561 was detected at 2.62 min, yielding fragment ions at $m/z$ 449.1455, 327.1084, and 165.0487. The product ion $m/z$ 449.1455 was determined to have the molecular formula $C_{22}H_{26}O_{10}$, indicating a loss of 30 Da compared to the precursor ion, which suggested the elimination of a molecular CHOH from the glucose moiety. Subsequent fragmentation involved the loss of a benzoyl group, resulting in the formation of the ion at $m/z$ 327.1084. The characteristic product ion at $m/z$ 165.0487 was inferred to be $[M-H-CH_2O-Benzoyl-C_6H_{10}O_5]^-$, and this fragment originated from the pinane basic framework intrinsic to the monoterpene glycosides (Figure 10A). It showed similar fragmentation pathways with reference standard paeoniflorin [43]. Therefore, we defined the compound as paeoniflorin. The precursor ion peak of the compound with a RT of 3.53 min is $m/z$ 631.1666 $[M-H]^-$. Based on the elemental composition, its possible molecular formula is inferred to be $C_{30}H_{32}O_{15}$. Furthermore, the fragment ions are generated from the parent ion through the sequential loss of neutral fragments: $m/z$ 509.1303 $[M-H-C_7H_6O_2]^-$, 313.0561 $[M-H-C_7H_6O_2-C_{10}H_{12}O_4]^-$, 255.0662 $[M-H-C_7H_6O_2-C_{10}H_{12}O_4-C_2H_2O_2]^-$, 169.0137 $[M-H-C_7H_6O_2-C_{10}H_{12}O_4-C_2H_2O_2-C_3H_2O_3]^-$ were observed. The fragment ions are assigned as follows: the ion at $m/z$ 509.1303 $[M-H-C_7H_6O_2]^-$ is generated from the parent ion by the loss of a benzoic acid. Subsequently, the further loss of the pinane nucleus yields the fragment ion at $m/z$ 313.0561 $[M-H-C_7H_6O-C_{10}H_{12}O_4]^-$. The galloyl glucose residues then undergo cleavage and rearrangement, losing a molecule of $C_2H_2O_2$ to produce the fragment at $m/z$ 225.0662 $[M-H-C_7H_6O_2-C_{10}H_{12}O_4-C_2H_2O_2]^-$. Finally, the loss of a molecule of $C_3H_2O_3$ produces the characteristic gallic acid fragment ion at $m/z$ 169.0137 $[M-H-C_7H_6O_2-C_{10}H_{12}O_4-C_2H_2O_2-C_3H_2O_3]^-$. Based on its characteristic secondary fragmentation data and mass spectral behavior, compound **26** was identified

as galloylpaeoniflorin [43]. The fragmentation pathway in negative ion mode is shown in Figure 10B.

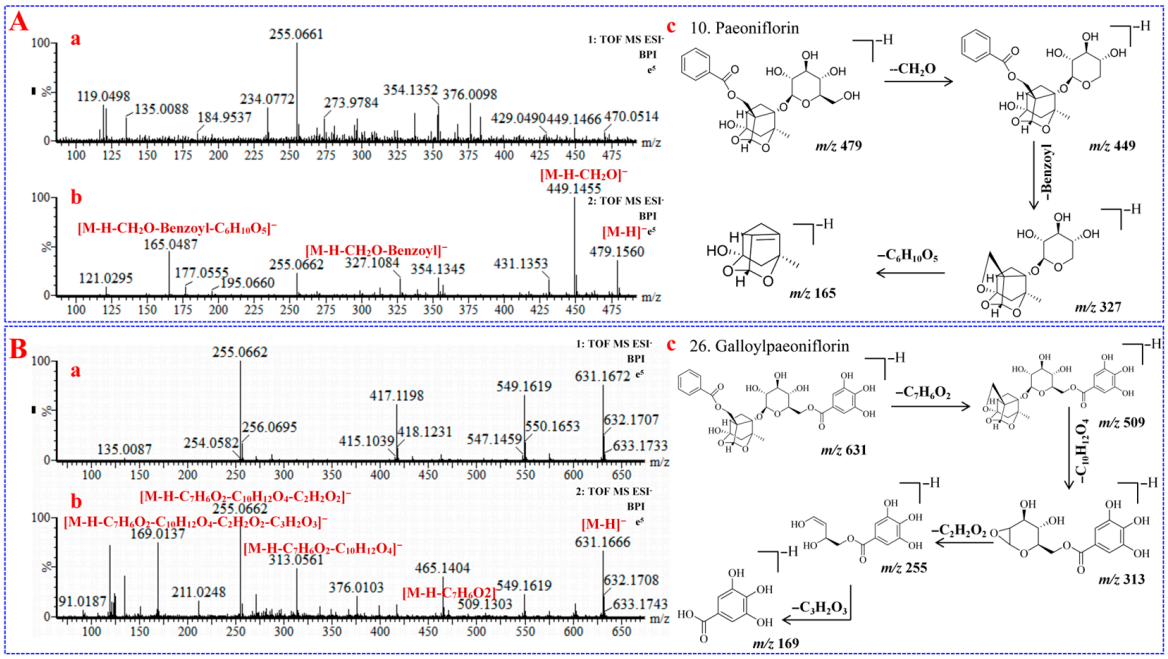



**Figure 10.** The MS1 (**a**), MS2 spectra (**b**) and characteristic fragmentation pathways (**c**) of paeoniflorin (**A**) and galloylpaeoniflorin (**B**).

### 2.2.4. Characterization of Organic Acids Constituents in HQD

Organic acids, as core components of natural products, not only participate in energy metabolism within biological systems but also exhibit a variety of bioactivities, including antioxidant, antibacterial, and anti-inflammatory functions [44]. The presence of characteristic functional groups such as carboxyl and hydroxyl groups within their molecular structures results in distinct fragmentation patterns during mass spectrometric analysis, including the elimination of carboxyl groups and the cleavage of aromatic ring moieties. These characteristic fragmentation pathways are not only valuable for compound identification but also provide crucial insights into the mechanisms underlying their bioactivities. The *p*-Hydroxybenzene propanoic acid was used to illustrate the identification process (Figure 11). The precursor ion $[M-H]^-$ observed at $m/z$ 165.0556 at 2.40 min, yields a characteristic fragment ion at $m/z$ 121.0293 through the loss of $CO_2$ (44 Da). This decarboxylation is a characteristic fragmentation pathway for aromatic carboxylic acids [45]. Based on this fragmentation pattern, together with retention time and literature comparison, compound **7** was putatively annotated as *p*-hydroxybenzene propanoic acid.

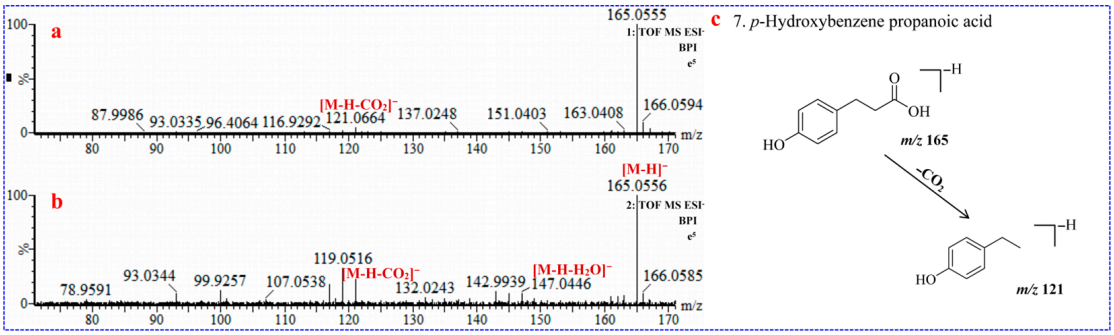



**Figure 11.** The MS1 (**a**), MS2 spectra (**b**) and characteristic fragmentation pathways (**c**) of *p*-Hydroxybenzene propanoic acid.

## 3. Discussion

The off-line 2D LC and UHPLC-QTOF/MS strategy established in this study effectively overcame the challenge in comprehensive component profiling of complex traditional Chinese prescription HQD—the masking of trace components by dominant constituents. It is worth noting that the off-line 2D LC and UHPLC-QTOF/MS strategy proposed in this study offers significant advantages for elucidating the comprehensive chemical profile of complex TCPs characterized by complex compositions and large disparities in component content. However, its application may be limited for samples that already exhibit sufficient detection sensitivity using conventional injection analysis. Compared with the traditional analytical strategy, this strategy significantly improved the detection sensitivity of trace components, successfully identifying 192 compounds, including 88 flavonoids, 80 triterpenoids, 7 monoterpene glycosides, 3 fatty acid amides, 3 phenylethanoid glycosides, 4 coumarins, 3 saccharides, 1 organic acid, and 3 others, a substantial supplement from previous studies. The identification of these compounds provides a foundation for understanding the chemical basis of HQD's pharmacological activities. However, it was important to acknowledge the limitations and confidence levels associated with these identifications. Following the MSI guidelines, of the 192 compounds characterized in this study, **11** compounds were identified at confidence Level 1 through comparison with reference standards using retention time and MS/MS fragmentation pattern matching. A total of 146 compounds were assigned Level 2.1 based on matching with publicly or commercially available MS/MS spectral libraries, while **15** compounds were assigned Level 2.2 based on characteristic product ions and neutral losses, supported by structure elucidation tools and network analysis. While Level 2 identifications provided valuable information for chemical profiling, they should be considered tentative pending confirmation with certified reference standards.

It was noteworthy that this study successfully differentiated some isomeric compounds in HQD based on characteristic mass spectrometric fragmentation ions and differences in reversed-phase chromatographic retention behavior. By elucidating the cleavage rules of positional isomers of functional groups and glycosyl linkage positions in flavonoid glycosides, some flavonoid glycoside isomers in HQD were distinguished. Specifically, 7-*O*-glycosides underwent direct heterolytic cleavage of the glycosidic bond due to the absence of a neighboring proton source, characterized by the neutral loss of 176 Da, whereas 8-*O*-glycosides, through intramolecular proton transfer driven by the adjacent phenolic hydroxyl group, triggered a sugar ring rearrangement leading to the preferential neutral loss of 148 Da. The flavanone glycosides are typically characterized by the RDA cleavage, resulting in the characteristic fragment ion $m/z$ 135 $[C_8H_7O_2]^-$. The chalcone glycosides are typically characterized by the β-fragmentation and rearrangement of the enone framework, generating the characteristic ion $m/z$ 147 $[C_9H_7O_2]^-$. The triterpenoid saponins in HQD were primarily represented by oleanane-type pentacyclic triterpenoid saponins derived from GRR. Different isomers could be inferred by observing characteristic fragmentation pathways of their aglycones, such as decarboxylation ($-CO_2$) and hydroxymethyl rearrangement loss ($-CH_2O$) [46]. These regularities provided support for clarifying the complex component groups in HQD. However, for those isomeric pairs that exhibited highly similar fragmentation pathways or lacked characteristic fragment ions, definitive characterization and identification could not be achieved with the current methodology. Future research could integrate additional orthogonal techniques to address this challenge.

The comprehensive chemical profiling conducted in this study provided a solid foundation for understanding the "holistic view" and synergistic effects underlying HQD. The results demonstrated that the chemical constituents of HQD were predominantly

flavonoids and triterpenoids. Among these, albiflorin, paeoniflorin, baicalin, wogonoside, wogonin, baicalein, and glycyrrhizic acid were identified as the seven principal components with the highest content, confirmed at MSI Level 1. Flavonoids exhibited significant anti-inflammatory, antibacterial, and antioxidant activities, contributing to heat-clearing and detoxification, while triterpenoids displayed anti-inflammatory and immunomodulatory functions. Beyond these major constituents, the pharmacological significance of many trace components identified in this study warrants consideration. For example, fatty acid amides are known to function as endogenous signaling molecules with anti-inflammatory and immunomodulatory properties [47–49]. Specifically, stearamide (compound **187**) modulates membrane stability and immune function through mechanisms distinct from flavonoid-mediated COX-2 inhibition. Erucamide (compound **191**) exhibits significant antisecretory effects in intestinal models, while also upregulating anti-inflammatory cytokines (IL-6, TNF-α) in myeloid cells, thereby complementing the anti-inflammatory actions of baicalin and glycyrrhizic acid. Docosanamide (compound **192**) has been characterized as an angiogenic lipid with potential roles in tissue repair, aligning with HQD's cooling-blood effects. Although present at low abundance, these fatty acid amides may contribute to the formula's heat-clearing and detoxifying effects through mechanisms distinct from those of the major flavonoids and triterpenoids. Similarly, trace phenolic acids, such as p-hydroxybenzene propanoic acid (compound **7**), have been reported to exhibit antioxidant and anti-inflammatory activities [50,51], potentially augmenting the overall efficacy of HQD. Collectively, the chemical components of HQD exhibit substantial diversity, ranging from abundant flavonoids and triterpenoids to trace fatty acid amides and phenolic acids. The complexity of their functional networks underpins the multi-target integrated regulation achieved through the emperor-minister-adjuvant-courier compatibility principle. This compositional and mechanistic complexity constitutes the basis for the core efficacy of the prescription in clearing heat, drying dampness, cooling blood, and relieving diarrhea.

## 4. Materials and Methods

### *4.1. Reagents, Chemicals, and Plant Materials*

LC/MS-grade acetonitrile, formic acid and HPLC-grade acetonitrile were purchased from Thermo Fisher Scientific (Thermo Fisher, Waltham, MA, USA). Distilled water was obtained from Watson's Food & Beverage Co., Ltd. (Guangzhou, China). Other analytical-grade reagents were procured commercially from Sinopharm Chemical Reagent Co., Ltd. (Beijing, China).

SR, PL, GRR, and JF were sourced from Shanxi, Inner Mongolia, and Shandong respectively, with batch numbers 2309044, 2312075, 2304043, and 2401124 in sequence. A total of 11 compounds (purity > 98%), involving baicalin (1), baicalein (2), wogonin (3), wogonoside (4), oroxylin A (5), apigenin (6), liquiritin (7), glycyrrhizic acid (8), paeoniflorin (9), albiflorin (10), galloylpaeoniflorin (11) used as the reference compounds were purchased from Shanghai yuanye Bio-Technology Co., Ltd. (Shanghai, China) or Shanghai Acmec Biochemical Technology Co., Ltd. (Shanghai, China).

### *4.2. Preparation of Sample Solutions*

The SR, PRR, GRR, and JF were ground to a fine powder (<40 mesh). Precisely weighed quantities of 12 g of SR powder, 8 g of PRR powder, 8 g of GRR powder, and 8 g of JF powder were placed in a 250 mL round-bottom flask. Eight times the weight of the powders of 50% ethanol ($v/v$) was added, and the mixture was subjected to heating reflux extraction once for 2 h. After filtration, the residue was then subjected to a second heating reflux extraction with eight times the weight of the powders of 50% ethanol

for 2 h, and the two filtrates were combined. The extracted solution was then concentrated under reduced pressure (maintaining a temperature below 45 °C) until a dry residue was obtained. Subsequently, 100 mg of the concentrated extract was re-dissolved in 5 mL of 50% ethanol, filtered through a 0.22 μm filter, and the resulting filtrate was collected for further analysis.

### *4.3. Sample Preparation*

The $^{1}$D LC system used in this work was the Thermo Scientific Vanquish Core Analytical Purification System (Thermo Fisher Scientific, USA), which integrates a valve-based VFC into the high-performance Vanquish Core HPLC platform. The integrated platform enables the execution of a complete workflow—from method development and sample analysis to target fraction collection—within a single system. First, the elution conditions were systematically optimized to ultimately establish the following preparative conditions: an Agilent ZORBAX SB-C18 column (4.6 mm × 250 mm, 5 μm) was employed for separation, with the column oven temperature maintained at 35 °C. The mobile phase consisted of eluent A (0.1% formic acid in water) and eluent B (0.1% formic acid in acetonitrile), utilizing a gradient program as follows: 0−10 min, 15−20% B; 10−15 min, 20−23% B; 15−45 min, 23−23% B; 45−50 min, 23−35% B; 50−70 min, 35−35% B; 70−74 min, 35−95% B; 74−76 min, 95−95% B; 76−77 min, 95−15% B; and 77−80 min, 15−15% B, with a flow rate of 1.0 mL/min. The autosampler was set at 18 °C for optimal performance. The injection volume was 100 μL, the injection was repeated 45 times, and the UV detection wavelengths were set at 210 nm and 365 nm. The CAD operated with a collection frequency of 10 Hz, an evaporation temperature of 35 °C, and a filter time of 1 s. The chromatographic peaks with RTs of 8.10−8.75 min, 9.35−9.95 min, 24.20−25.50 min, 31.75−32.75 min, 37.5−39.00 min, 44.50−46.50 min, and 65.00−66.00 min were removed. The sample eluent was collected and simultaneously concentrated to dryness under reduced pressure, with the distillation temperature controlled not to exceed 45 °C, re-dissolved in 50% ethanol, filtered through a 0.22 μm filter, and the subsequent filtrate was obtained.

### *4.4. UHPLC-Q-TOF/MS Analysis Conditions*

The $^{2}$D UHPLC-Q-TOF/MS analysis was performed using the Waters ACQUITY UPLC system equipped with Synapt G2-S mass spectrometry (Waters Corp., Milford, MA, USA). A Waters ACQUITY BEH C18 column (2.1 × 100 mm, 1.7 μm, USA) maintained at 35 °C was used for chromatographic separation. The mobile phase system comprised water with 0.1% formic acid (A) and acetonitrile (B), with a 0.4 mL/min flow rate. The gradient was set as follows: 0–2 min, 5–21% B; 2–11 min, 21–32% B; 11–20 min, 32–42% B; 20–23 min, 42–80% B; 23–25 min, 80–95% B; 25–27 min, 95–95% B; 27–28 min, 95–5% B; 28–30 min, 5–5% B. The autosampler temperature was set at 18 °C. The injection volume was 1 μL.

High-accuracy mass spectrometric data were recorded using the QTOF mass spectrometer in both positive and negative electrospray ionization (ESI) modes employing the $MS^{E}$. The LockSpray ion source was configured with optimized parameters: mass range of $m/z$ 100–1200, scan time of 0.2 s, source temperature set to 120 °C, desolvation gas temperature at 450 °C, cone gas flow ($N_2$) of 50 L/h, desolvation gas flow ($N_2$) at 850 L/h, cone voltage at 30 V, and capillary voltage of 3.0 kV for positive ion mode and −2.5 kV for negative ion mode. In $MS^{E}$ mode, the low collision energy was set to 6.0 eV, with the high collision energy ramp ranging from 35 to 55 eV for $ESI^{+}$ analysis and 30 to 50 eV for $ESI^{-}$ analysis. Ultra-high purity argon (Ar, purity ≥ 99.997%) was used as the collision-induced dissociation (CID) gas for all MS/MS experiments. To ensure mass accuracy and reproducibility, leucine-enkephalin was utilized as the lock mass, with $m/z$

values of 556.2766 in positive ion mode and 554.2620 in negative ion mode, respectively. The mass spectrometer was operated at a working resolution of 50,000~60,000 FWHM (full width at half maximum) for both positive and negative ion modes.

### *4.5. Date Processing and Analysis*

The acquired MS data were analyzed using Masslynx (Version 4.1, Waters Corp.), while UHPLC-CAD data were processed with Chromeleon 7 software (Version 4.1 Thermo Fisher Scientific, USA). An in-house database was established to compile the primary published phytochemical constituents (including compound name, molecular formula, exact mass, structure, and MS fragmentation) found in the four herbs of HQD. This was accomplished by exploring the TCMID platform (https://ngdc.cncb.ac.cn/databasecommons/database/id/437, accessed between 5 November 2025 and 30 December 2025), TCMSP databases (https://www.tcmsp-e.com/load_intro.php?id=43, accessed between 5 November 2025 and 30 December 2025), and supplemented by the relevant literature from PubMed, Web of Science, and CNKI (https://www.cnki.net/, accessed between 5 November 2025 and 30 December 2025). The fragment ion information obtained from reference standard analysis was summarized, and the structurally relevant fragments were designated as characteristic fragments and neutral loss fragments, respectively. The adduct ions were set as $[M-H]^-$, $[M-H_2O-H]^-$, and $[M+HCOO]^-$ in negative ion mode, while $[M+H]^+$ and $[M+Na]^+$ were used in positive ion mode.

The confidence levels for the characterization of these components are defined according to the MSI as follows: Level 1: structure confirmed by comparison with a standard; 2.1: structure annotated based on publicly or commercially available MS/MS spectral libraries; 2.2: structure putatively annotated using characteristic product ions and neutral losses, supported by structure elucidation tools and network analysis.

## 5. Conclusions

This study developed and applied an off-line 2D LC and UHPLC-QTOF/MS strategy for the in-depth chemical profiling of HQD, a complex TCP characterized by diverse constituents and significant variations in component content. This strategy enabled the characterization of 192 compounds in HQD, including 88 flavonoids, 80 triterpenoids, 7 monoterpene glycosides, 3 fatty acid amides, 3 phenylethanoid glycosides, 4 coumarins, 3 saccharides, 1 organic acid, and 3 others. Compounds were classified according to MSI confidence levels, with 11 compounds confirmed at Level 1 using reference standards, 146 annotated at Level 2.1 via spectral library matching, and 15 putatively annotated at Level 2.2 based on characteristic fragmentation patterns. While 99 compounds could be identified using a traditional analytical strategy, our approach enabled the detection of 192 peaks in the base peak chromatogram. Notably, this study successfully differentiated isomers of flavonoid glycosides and triterpenoid saponins based on their diagnostic fragmentation behaviors. Flavonoid glycoside isomers were distinguished by characteristic neutral losses, while flavanones and chalcones were identified through RDA cleavage and β-rearrangement, respectively. Furthermore, isomers of triterpenoid saponins were inferred via aglycone-specific fragmentation pathways.

**Supplementary Materials:** The following supporting information can be downloaded at: https://www.mdpi.com/article/10.3390/separations13040110/s1. Figure S1: The UHPLC-CAD chromatograms of HQD. (A): the injection volume is 1 μL, and the response signal has not undergone amplification processing, (B): the injection volume is 1 μL, and the response signal has undergone amplification processing, (C): the injection volume is 10 μL, and the response signal has undergone amplification processing; Figure S2: Optimization of chromatographic conditions for HQD. (A) Comparison of different chromatographic columns (a for YMC-Triart C18, b for NanoChrom

ChromCore Phenyl, c for COSMOSIL 5C18-AR-II, d for Agilent ZORBAX SB-C18). (B) Comparison of elution conditions on an Agilent ZORBAX SB-C18 column (c for the optimal elution condition). The main seven constituents are indicated by red dots in Figure S3. The number of annotated compounds of HQD in the UHPLC-Q-TOF/MS chromatogram before and after $^{1}$D LC system processing; Figure S4. Comparison of Q-TOF peak areas for trace-level components **19**, **21**, **49**, **63**, **76**, **93**, **101**, **130**, and **175** of different structural types before and after $^{1}$D LC system processing; Figure S5. The prepared chromatogram of the sample's repeated injection in the $^{1}$D LC system. Table S1. Identification of 192 compounds in HQD by UHPLC-QTOF/MS in positive and negative ion modes; Table S2. Relative standard deviations (RSDs) of retention times (RTs) and peak areas for peaks 1~7 in replicate injections. Table S3. Stability recovery of representative compounds during repeated injections and concentration.

**Author Contributions:** Conceptualization, X.T.; methodology, Y.F., H.L. and B.M.; software, J.Z.; validation, X.T., X.C. and J.S.; formal analysis, H.L.; investigation, X.C. and J.S.; resources, Y.N.; data curation, B.M.; writing—original draft preparation, Y.F.; writing—review and editing, Y.F., H.L. and Y.N.; visualization, J.Z.; supervision, Y.N.; project administration, B.M.; funding acquisition, B.M. All authors have read and agreed to the published version of the manuscript.

**Funding:** This work was funded by the National Key Research and Development Program of China (2023YFC3502804).

**Institutional Review Board Statement:** Not applicable.

**Informed Consent Statement:** Not applicable.

**Data Availability Statement:** The original contributions presented in this study are included in the article. Further inquiries can be directed to the corresponding authors.

**Acknowledgments:** The authors have reviewed and edited the output and take full responsibility for the content of this publication.

**Conflicts of Interest:** The authors declare no conflicts of interest.

## Abbreviations

The following abbreviations are used in this manuscript:

| | |
|---|---|
| TCPs | traditional Chinese prescriptions |
| TCM | traditional Chinese medicine |
| HQD | Huangqin decoction |
| SR | Scutellariae Radix |
| PRR | Paeoniae Radix Rubra |
| GRR | Glycyrrhizae Radix et Rhizoma |
| JF | Jujubae Fructus |
| CAD | charged aerosol detector |
| VFC | vanquish fraction collector |
| UV | ultraviolet |
| UHPLC-Q-TOF/MS | ultra-high performance liquid chromatography-quadrupole time-of-flight mass spectrometry |
| ESI | electrospray ionization |
| BPI | base peak ion |
| RT | retention time |
| CID | collision-induced dissociation |
| FWHM | full width at half maximum |

## References

1. Wang, Z.B.; Tang, W.; Tong, K.; Huang, W.J.; Chen, B.B.; Qiao, S.J.; Han, H.R.; Li, X.D.; Wang, Y. Thinking on compatibility of prescription and drugs based on perspective of combination of disease, syndrome, and symptom. *J. Beijing Univ. Tradit. Chin. Med.* **2024**, *47*, 929–933.

2. Ding, Y.; Hong, Y.L.; Qi, F.J.; Gan, S.Y.; Wang, Z.J.; Zuo, X.H.; Zhao, Y. The innovative application of "Jun (emperor)—Chen (minister)—Zuo (adjuvant)—Shi (courier)" in clinical practice. *Lishizhen Med. Mater. Medica Res.* **2022**, *33*, 1178–1179. [CrossRef]
3. Liu, L.W.; Tang, M.; Zhang, Z.B.; Zhou, P.P.; Xue, L.P.; Jia, Q.Q.; Zhao, L.G.; Zuo, L.H.; Sun, Z. A stepwise integrated strategy to explore quality markers of Qishen Yiqi dripping pills against myocardial ischemia. *Phytomedicine* **2024**, *135*, 156182. [CrossRef]
4. Wang, X.; Zhang, X.; Li, J.; Fu, J.; Zhao, M.; Zhang, W.; Weng, W.; Li, Q. Network pharmacology and LC-MS approachs to explore the active compounds and mechanisms of Yuanjiang decoction for treating bradyarrhythmia. *Comput. Biol. Med.* **2023**, *152*, 106435. [CrossRef]
5. Guo, T.J.; Yuan, X.; Zou, Y.H.; Li, H.J.; Chen, Y.H.; Qing, Y.; Zheng, Y.F.; Liao, W. Modern research progress on classic formula Huangqin Decoction. *Chin. Tradit. Herb. Drugs* **2025**, *56*, 1414–1427.
6. Wang, L.F. Research progress on classical prescription of Huangqin Decoction. *Chin. Med. Mod. Distance Educ. China* **2020**, *18*, 191–194. [CrossRef]
7. Gu, S.H.; He, M.; Zhu, R.H.; Li, L.; Zhang, T. Historical evolution and key information research of classic Chinese formula Huangqin Decoction. *Shanghai J. Tradit. Chin. Med.* **2024**, *58*, 23–30. [CrossRef]
8. Wang, E.; Bussom, S.; Chen, J.G.; Quinn, C.; Bedognetti, D.; Lam, W.; Guan, F.; Jiang, Z.; Mark, Y.; Zhao, Y.D.; et al. Interaction of a traditional Chinese medicine (PHY906) and CPT-11 on the inflammatory process in the tumor microenvironment. *BMC Med. Genom.* **2011**, *4*, 38. [CrossRef]
9. Lam, W.; Jiang, Z.; Guan, F.; Hu, R.; Liu, S.H.; Chu, E.; Cheng, Y.C. The number of intestinal bacteria is not critical for the enhancement of antitumor activity and reduction of intestinal toxicity of irinotecan by the Chinese herbal medicine PHY906 (KD018). *BMC Complement. Altern. Med.* **2014**, *14*, 490. [CrossRef]
10. Lam, W.; Bussom, S.; Guan, F.; Jiang, Z.; Zhang, W.; Gullen, E.A.; Liu, S.H.; Cheng, Y.C. The four-herb Chinese medicine PHY906 reduces chemotherapy-induced gastrointestinal toxicity. *Sci. Transl. Med.* **2010**, *2*, 45–59. [CrossRef]
11. Lam, W.; Jiang, Z.; Guan, F.; Huang, X.; Hu, R.; Wang, J.; Bussom, S.; Liu, S.H.; Zhao, H.; Yen, Y.; et al. PHY906(KD018), an adjuvant based on a 1800-year-old Chinese medicine, enhanced the anti-tumor activity of Sorafenib by changing the tumor microenvironment. *Sci. Rep.* **2015**, *5*, 9384. [CrossRef]
12. Yang, X.; Lam, W.; Jiang, Z.; Guan, F.; Han, X.; Hu, R.; Cai, W.; Cheng, W.; Liu, S.H.; Cheng, P.; et al. YIV-906 potentiated anti-PD1 action against hepatocellular carcinoma by enhancing adaptive and innate immunity in the tumor microenvironment. *Sci. Rep.* **2021**, *11*, 13482. [CrossRef]
13. Lam, W.; Hu, R.; Liu, S.H.; Cheng, P.; Cheng, Y.C. YIV-906 enhances nuclear factor of activated T-cells (NFAT) activity of T cells and promotes immune checkpoint blockade antibody action and CAR T-cell activity. *Front. Pharmacol.* **2023**, *13*, 1095186. [CrossRef]
14. Li, M.X.; Li, M.Y.; Lei, J.X.; Wu, Y.Z.; Li, Z.H.; Chen, L.M.; Zhou, C.L.; Su, J.Y.; Huang, G.X.; Huang, X.Q.; et al. Huangqin decoction ameliorates DSS-induced ulcerative colitis: Role of gut microbiota and amino acid metabolism, mTOR pathway and intestinal epithelial barrier. *Phytomedicine* **2022**, *100*, 154052. [CrossRef]
15. Huang, S.; He, J.; Chen, Y.; Wang, X.; Li, Y.; Su, Y.; Wen, R.; Li, X.; Yang, G.; Luo, S.; et al. Effect of Huangqin decoction on regulating intestinal flora in colitis mice characterized as inhibition of the NOD2-dependent pathway. *Pharm. Biol.* **2022**, *60*, 108–118. [CrossRef]
16. Li, M.Y.; Li, M.X.; Xu, N.; Li, Z.H.; Zhang, Y.M.; Gan, Y.X.; Luo, H.J.; Zhou, C.L.; Liu, Y.H.; Su, Z.R.; et al. Effects of Huangqin Decoction on ulcerative colitis by targeting estrogen receptor alpha and ameliorating endothelial dysfunction based on system pharmacology. *J. Ethnopharmacol.* **2021**, *271*, 113886. [CrossRef] [PubMed]
17. Wang, D.; Ma, X.; Guo, S.; Wang, Y.; Li, T.; Zou, D.; Song, H.; Yang, W.; Ge, Y. Effect of Huangqin Tang on urine metabolic profile in rats with ulcerative colitis based on UPLC-Q-Exactive Orbitrap MS. *Evid.-Based Complement. Altern. Med.* **2020**, *2020*, 1874065. [CrossRef]
18. Yan, B.F.; Pan, L.F.; Quan, Y.F.; Sha, Q.; Zhang, J.Z.; Zhang, Y.F.; Zhou, L.B.; Qian, X.L.; Gu, X.M.; Li, F.T.; et al. Huangqin decoction alleviates lipid metabolism disorders and insulin resistance in nonalcoholic fatty liver disease by triggering Sirt1/NF-κB pathway. *World J. Gastroenterol.* **2023**, *29*, 4744–4762. [CrossRef]
19. Yan, B.F.; Wang, Y.; Wang, W.B.; Ding, X.J.; Wei, B.; Liu, S.J.; Fu, T.M.; Chen, L.; Zhang, J.Z.; Liu, J.; et al. Huangqin decoction mitigates hepatic inflammation in high-fat diet-challenged rats by inhibiting TLR4/NF-κB/NLRP3 pathway. *J. Ethnopharmacol.* **2023**, *303*, 115999. [CrossRef]
20. Wang, J.; Li, R.; Zhang, M.; Gu, C.; Wang, H.; Feng, J.; Bao, L.; Wu, Y.; Chen, S.; Zhang, X. Influence of Huangqin Decoction on the immune function and fecal microbiome of chicks after experimental infection with Escherichia coli O78. *Sci. Rep.* **2022**, *12*, 16632. [CrossRef]
21. Xu, X.; Fang, C.; Wang, Y.; Lu, F.; Liu, S. Integrating network pharmacology and metabolomics to elucidate the mechanism of action of Huang Qin Decoction for treament of diabetic liver injury. *Front. Pharmacol.* **2022**, *13*, 899043. [CrossRef]

22. Gao, L.; Zhang, A.P.; Fu, L.; Li, Q.W.; Qin, X.M.; Zhao, J. Huangqin decoction attenuates spared nerve injury (SNI)-induced neuropathic pain by modulating microglial M1/M2 polarization partially mediated by intestinal nicotinamide metabolism. *Phytomedicine* **2024**, *129*, 155594. [CrossRef]
23. Gao, L.; Cao, M.; Du, G.H.; Qin, X.M. Huangqin Decoction exerts beneficial effects on rotenone-induced rat model of Parkinson's disease by improving mitochondrial dysfunction and alleviating metabolic abnormality of mitochondria. *Front. Aging Neurosci.* **2022**, *14*, 911924. [CrossRef] [PubMed]
24. Schilling, K.; Holzgrabe, U. Recent applications of the charged aerosol detector for liquid chromatography in drug quality control. *J. Chromatogr. A* **2020**, *1619*, 460911. [CrossRef]
25. Wu, L.; Gong, X.; Qu, H. An optimization strategy for charged aerosol detection to linearize the detector response in the multicomponent quantitative analysis of Qishen Yiqi dripping pills. *J. Sep. Sci.* **2024**, *47*, e2300784. [CrossRef]
26. Rosentreter, U.; Huber, U. Optimal fraction collecting in preparative LC/MS. *J. Comb. Chem.* **2004**, *6*, 159–164. [CrossRef] [PubMed]
27. Song, J.; Liu, S.; Sun, M.; Tu, G.; Zhang, Z.; Liu, Y.; Nan, Y.; Shen, G.; Chen, X.; Liang, H.; et al. Isolation and structural elucidation of immunomodulatory oligosaccharides from Trillium tschonoskii. *Glycoconj. J.* **2026**, *43*, 8. [CrossRef] [PubMed]
28. Yao, L.; Wang, X.; Nan, Y.; Liang, H.Z.; Wang, M.Y.; Song, J.; Chen, X.J.; Ma, B.P. Exploring the chemical compositions of Fufang Yinhua Jiedu granules based on ultra-high-performance liquid chromatography coupled to quadrupole time-of-flight mass spectrometry combined with multistage intelligent data annotation strategy. *J. Chromatogr. A* **2024**, *1728*, 465010. [CrossRef]
29. Wang, X.; Wu, H.; Li, M.; Guo, X.; Cheng, X.; Jing, W.; Wei, F. A comprehensive analysis of Fel Ursi and its common adulterants based on UHPLC-QTOF-MSE and chemometrics. *Molecules* **2024**, *29*, 3144. [CrossRef]
30. Sun, Z.R.; Jia, D.; Chen, X.F.; Chai, Y.F. Identification on components of Huangqin Tang and rats blood components after administration based on UHPLC-QTOF MS analysis. *J. Instrum. Anal.* **2023**, *42*, 960–967. [CrossRef]
31. Tang, X.; Cui, Y.; Feng, B. The chemical constituents and metabolite profiles of Huangqin decoction in normal and ulcerative colitis rats by UHPLC-Q-TOF/MS analysis. *J. Pharm. Biomed. Anal.* **2024**, *237*, 115763. [CrossRef]
32. Jia, L.Y.; Zheng, F.Y.; Ma, Y.; Zhang, Y.F. Studies on chemical composition, pharmacological effect, clinical application of Huangqin Decoction and its quality marker prediction analysis. *J. Liaoning Univ. Tradit. Chin. Med.* **2025**, *27*, 149–156. [CrossRef]
33. Teng, X.; Wu, B.; Liang, Z.; Zhang, L.; Yang, M.; Liu, Z.; Liang, Q.; Wang, C. Three bioactive compounds from Huangqin decoction ameliorate Irinotecan-induced diarrhea via dual-targeting of Escherichia coli and bacterial β-glucuronidase. *Cell Biol. Toxicol.* **2024**, *40*, 88. [CrossRef]
34. Wu, Y.; Liu, X.; Li, G. Integrated bioinformatics and network pharmacology to identify the therapeutic target and molecular mechanisms of Huangqin decoction on ulcerative Colitis. *Sci. Rep.* **2022**, *12*, 159. [CrossRef] [PubMed]
35. Zhang, B.W.; Dong, Y.S.; Yu, N.; Sun, Y.M.; Xing, Y.; Yang, F.; Yua, X.X.; Sun, W.L.; Sun, J.; Lia, X.; et al. Intestinal metabolism of baicalein after oral administration in mice: Pharmacokinetics and mechanisms. *J. Funct. Foods* **2019**, *54*, 53–63. [CrossRef]
36. Łukasz, M.; Maciej, S.; Michał, J.; Wieslaw, O.; Piotr, K. Fragmentation pathways of acylated flavonoid diglucuronides from leaves of Medicago truncatula. *Phytochem. Anal.* **2010**, *21*, 224–233. [CrossRef]
37. Zhu, H.D.; Tian, P.; Guan, L.J.; Chen, L.M.; Liu, X.Q.; Gao, H.M.; Wang, Z.M. Analysis and structural identification of relevant substances in Breviscapine for Injection. *Zhongguo Zhong Yao Za Zhi* **2020**, *45*, 1350–1356. [CrossRef]
38. Kitagawa, I.; Hori, K.; Uchida, E.; Chen, W.Z.; Yoshikawa, M.; Ren, J. Saponin and sapogenol. L. On the constituents of the roots of *Glycyrrhiza uralensis* Fischer from Xinjiang, China. Chemical structures of licorice-saponin L3 and isoliquiritin apioside. *Chem. Pharm. Bull.* **1993**, *41*, 1567–1572. [CrossRef]
39. Batiha, G.E.-S.; Beshbishy, A.M.; El-Mleeh, A.; Abdel-Daim, M.M.; Devkota, H.P. Traditional Uses, Bioactive Chemical Constituents, and Pharmacological and Toxicological Activities of *Glycyrrhiza glabra* L. (Fabaceae). *Biomolecules* **2020**, *10*, 352. [CrossRef] [PubMed]
40. Yang, R.; Yuan, B.C.; Ma, Y.S.; Zhou, S.; Liu, Y. The anti-inflammatory activity of licorice, a widely used Chinese herb. *Pharm. Biol.* **2017**, *55*, 5–18. [CrossRef]
41. Yin, R.; Yu, X.Y.; Wei, X.X.; Shi, C.Z.; Zhao, S.; Wang, X.; Sun, Y.F.; Han, F. Analysis of chemical components and components migrating to blood of Guizhi Gancao Decoction by UHPLC-Q-Exactive Orbitrap MS method. *Chin. Arch. Tradit. Chin. Med.* **2025**, *43*, 198–207. [CrossRef]
42. Yang, S.; Zhang, X.; Dong, Y.; Sun, G.; Jiang, A.; Li, Y. Cleavage rules of mass spectrometry fragments and rapid identification of chemical components of Radix Paeoniae Alba using UHPLC-Q-TOF-MS. *Phytochem. Anal.* **2021**, *32*, 836–849. [CrossRef] [PubMed]
43. He, X.; Wu, H.M.; Xiong, L.L.; Jin, H.L.; Liu, Y.F.; Shen, A.J.; Liang, X.M. Monoterpenoids from Paeoniae Radix Rubra based on UPLC-Q-TOF-MS. *China J. Chin. Mater. Medica* **2023**, *48*, 1005–1013. [CrossRef]
44. Ehteshami, S.; Abdollahi, F.; Ramezanian, A.; Rahimzadeh, M.; Dastjerdi, A.M. Maintenance of quality and bioactive compounds of cold stored pomegranate (*Punica granatum* L.) fruit by organic acids treatment. *Food Sci. Technol. Int.* **2021**, *27*, 151–163. [CrossRef] [PubMed]

45. Hossain, M.B.; Rai, D.K.; Brunton, N.P.; Martin-Diana, A.B.; Barry-Ryan, C. Characterization of phenolic composition in Lamiaceae spices by LC-ESI-MS/MS. *J. Agric. Food Chem.* **2010**, *58*, 10576–10581. [CrossRef] [PubMed]
46. Zheng, Y.F.; Qi, L.W.; Zhou, J.L.; Li, P. Structural characterization and identification of oleanane-type triterpene saponins in *Glycyrrhiza uralensis* Fischer by rapid-resolution liquid chromatography coupled with time-of-flight mass spectrometry. *Rapid Commun. Mass Spectrom.* **2011**, *24*, 3261–3270. [CrossRef]
47. Dang, H.T.; Kang, G.J.; Yoo, E.S.; Hong, J.; Choi, J.S.; Kim, H.S.; Chung, H.Y.; Jun, J.H. Evaluation of endogenous fatty acid amides and their synthetic analogues as potential anti-inflammatory leads. *Bioorganic Med. Chem.* **2011**, *19*, 1520–1527. [CrossRef]
48. Raboune, S.; Stuart, J.M.; Leishman, E.; Takacs, S.M.; Rhodes, B.; Basnet, A.; Jameyfield, E.; McHugh, D.; Widlanski, T.; Bradshaw, H.B. Novel endogenous N-acyl amides activate TRPV1-4 receptors, BV-2 microglia, and are regulated in brain in an acute model of inflammation. *Front. Cell. Neurosci.* **2014**, *8*, 195. [CrossRef]
49. Tahara, K.; Kobayashi, M.; Yoshida, S.; Onodera, R.; Inoue, N.; Takeuchi, H. Effects of cationic liposomes with stearylamine against virus infection. *Int. J. Pharm.* **2018**, *543*, 311–317. [CrossRef]
50. Zhang, Y.Y.; Li, X.L.; Li, T.Y.; Li, M.Y.; Huang, R.M.; Li, W.; Yang, R.L. 3-(4-Hydroxyphenyl)propionic acid, a major microbial metabolite of procyanidin A2, shows similar suppression of macrophage foam cell formation as its parent molecule. *Rsc Adv.* **2018**, *8*, 6242–6250. [CrossRef]
51. Kiriyama, Y.; Tokumaru, H.; Sadamoto, H.; Kobayashi, S.; Nochi, H. Effects of phenolic acids produced from food-derived flavonoids and amino acids by the gut microbiota on health and disease. *Molecules* **2024**, *29*, 5102. [CrossRef] [PubMed]


**Disclaimer/Publisher's Note:** The statements, opinions and data contained in all publications are solely those of the individual author(s) and contributor(s) and not of MDPI and/or the editor(s). MDPI and/or the editor(s) disclaim responsibility for any injury to people or property resulting from any ideas, methods, instructions or products referred to in the content.